Holomorphic lattice-motivated QCD coupling with zero IR limit and perturbative in the UV regime

Gorazd Cvetič (UTFSM, Valparaíso)

in collaboration with
César Ayala, Igor Kondrashuk, and Reinhart Kögerler
JPG44, 075001 [arXiv:1608.08240]; and arXiv:1703.01321, to appear in JPG

Loewe's 65 Fest, 5-7 December 2017, Santiago, Chile

Motivation for $\mathcal{A}(Q^2)$

In pQCD, $a(Q^2) \equiv \alpha_s(Q^2)/\pi$ ($Q^2 \equiv -q^2$) has Landau singularities, i.e., singularities at $0 < Q^2 \lesssim 0.1 \text{ GeV}^2$ ($-0.1 \text{ GeV}^2 < q^2 < 0$). This is a mathematical consequence of the pQCD truncated β-function RGE

$$Q^2 \frac{da(Q^2)}{dQ^2} = -\beta_0 a(Q^2)^2 \left[1 + c_1 a(Q^2) + c_2 a(Q^2)^2 + \cdots + c_N a(Q^2)^N \right] \tag{1}$$

- This contradicts the general principles of QFT for spacelike physical quantities $\mathcal{D}(Q^2)$, which require $\mathcal{D}(Q^2)$ to be analytic (holomorphic) in the complex Q^2-plane with the exception of part of the negative axis: $Q^2 \in \mathbb{C} \setminus (-\infty, -M_{\text{D,thr}}^2]$, where $M_{\text{D,thr}} \sim 0.1$ GeV.

- The Landau singularities of $a(Q^2)$ make the evaluation of TPS $\mathcal{D}(Q^2)_{\text{pt}} = a(Q^2) + \cdots + d_{N-1} a(Q^2)^N$ at low $|Q^2| \sim 1 \text{ GeV}^2$ very unreliable or simply impossible.

Motivation for $\mathcal{A}(Q^2)$

Another coupling $\mathcal{A}(Q^2)$ needs to replace $a(Q^2)$:

1. $\mathcal{A}(Q^2)$ is a holomorphic function for $Q^2 \in \mathbb{C} \backslash (-\infty, -M_{\mathrm{thr}}^2]$.

2. At high $|Q^2| \gg 1 \ \mathrm{GeV}^2$ we should have practically $\mathcal{A}(Q^2) = a(Q^2)$ (pQCD at high $|Q^2|$).

3. At intermediate $|Q^2| \sim 1 \ \mathrm{GeV}^2$, the $\mathcal{A}(Q^2)$-approach should reproduce the well measured semihadronic τ-decay physics.

4. At low $|Q^2| \lesssim 0.1 \ \mathrm{GeV}^2$, we should have $\mathcal{A}(Q^2) \sim Q^2$, as suggested by lattice results for the Landau gauge gluon and ghost propagators.

It turns out that the above property 1 will be a byproduct of the construction of $\mathcal{A}(Q^2)$ which should fulfill the above properties 2-4.

Construction of $\mathcal{A}(Q^2)$

In pQCD we have for $a(Q^2) \equiv \alpha_s(Q^2)/\pi$:

$$a(Q^2) = a(\Lambda^2) \frac{Z_{\mathrm{gl}}^{(\Lambda)}(Q^2) Z_{\mathrm{gh}}^{(\Lambda)}(Q^2)^2}{Z_1^{(\Lambda)}(Q^2)^2}, \tag{2}$$

where Z_{gl}, Z_{gh}, Z_1 are the dressing functions of the gluon and ghost propagator, and of the gluon-ghost-ghost vertex.

In the Landau gauge, $Z_1^{(\Lambda)}(Q^2) = 1$ to all orders (J.C.Taylor, 1971). Hence

$$\mathcal{A}_{\mathrm{latt.}}(Q^2) \equiv \mathcal{A}_{\mathrm{latt.}}(\Lambda^2) Z_{\mathrm{gl}}^{(\Lambda)}(Q^2) Z_{\mathrm{gh}}^{(\Lambda)}(Q^2)^2 . \tag{3}$$

$$\mathcal{A}_{\mathrm{latt.}}(Q^2) = \mathcal{A}(Q^2) + \Delta \mathcal{A}_{\mathrm{NP}}(Q^2) . \tag{4}$$

No finetuning at $Q^2 \to 0$ implies:

$$\Delta \mathcal{A}_{\mathrm{NP}}(Q^2) \sim Q^2 \qquad \text{and} \quad \mathcal{A}(Q^2) \sim Q^2 \qquad (Q^2 \to 0) \tag{5}$$
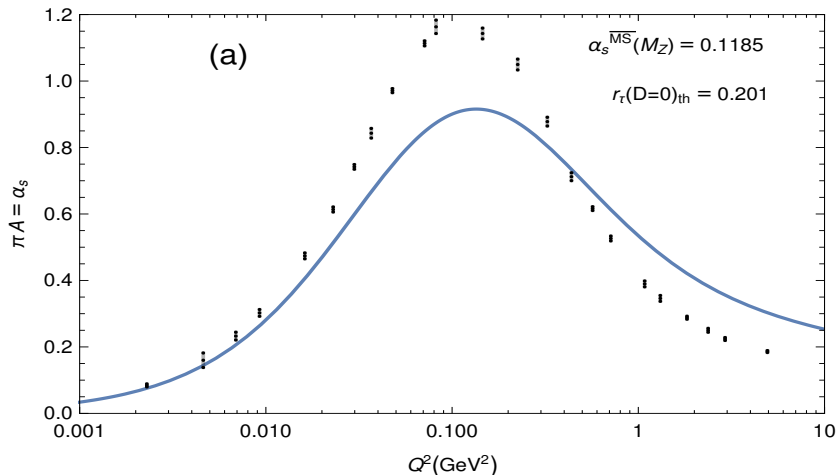
Figure: The $N_f = 0$ lattice values $\pi\mathcal{A}_{\text{latt.}}(Q^2)$ at low Q^2, from (Bogolubsky, Ilgenfritz, Müller-Preussker, Sternbeck [BIMS], 2009). The squared momenta are rescaled, from the MiniMOM (MM) lattice scheme scale to the usual $\overline{\text{MS}}$-like scale at $N_f = 0$. The solid curve is the ($N_f = 3$) theoretical coupling in the same IR regime (see later).

Construction of $\mathcal{A}(Q^2)$

The underlying pQCD coupling $a(Q^2)$ is in the same scheme up to 4-loops (G.C. and I.Kondrashuk, JHEP, 2011):

$$a(Q^2) = \frac{2}{c_1}\left[-\sqrt{\omega_2} - 1 - W_{\mp 1}(z) \right.$$
$$\left. + \sqrt{(\sqrt{\omega_2} + 1 + W_{\mp 1}(z))^2 - 4(\omega_1 + \sqrt{\omega_2})} \right]^{-1}, \qquad (6)$$

where $Q^2 = |Q^2| \exp(i\phi)$, W_{-1} Lambert function is used when $0 \leq \phi < \pi$, and W_{+1} when $-\pi \leq \phi < 0$, and

$$\omega_1 = c_2/c_1^2, \quad \omega_2 = c_3/c_1^3, \qquad z \equiv z(Q^2) = -\frac{1}{c_1 e}\left(\frac{\Lambda_L^2}{Q^2}\right)^{\beta_0/c_1}, \quad (7)$$

and the scheme coefficients are for Lambert MiniMOM (with $N_f = 3$):

$$c_2 = 9.2970(4.4711 \text{ in } \overline{\text{MS}}), \quad c_3 = 71.4538(20.9902 \text{ in } \overline{\text{MS}}) . \quad (8)$$

The world average (2014) $\alpha_s(M_Z^2; \overline{\text{MS}}) = 0.1185$ implies: $\Lambda_L = 0.1156$ GeV.

Construction of $\mathcal{A}(Q^2)$

The dispersive relation for $a(Q^2)$

$$a(Q^2) = \frac{1}{\pi} \int_{\sigma = -Q_{\mathrm{br}}^2 - \eta}^{\infty} \frac{d\sigma \rho_a(\sigma)}{(\sigma + Q^2)} \qquad (\eta \to +0), \qquad (9)$$

where $\rho_a(\sigma) \equiv \mathrm{Im}\, a(Q^2 = -\sigma - i\epsilon)$.

The dispersive relation for $\mathcal{A}(Q^2)$

$$\mathcal{A}(Q^2) = \frac{1}{\pi} \int_{\sigma = M_{\mathrm{thr}}^2 - \eta}^{\infty} \frac{d\sigma \rho_{\mathcal{A}}(\sigma)}{(\sigma + Q^2)} \qquad (\eta \to +0), \qquad (10)$$

where $\rho_{\mathcal{A}}(\sigma) \equiv \mathrm{Im}\, \mathcal{A}(Q^2 = -\sigma - i\varepsilon)$.
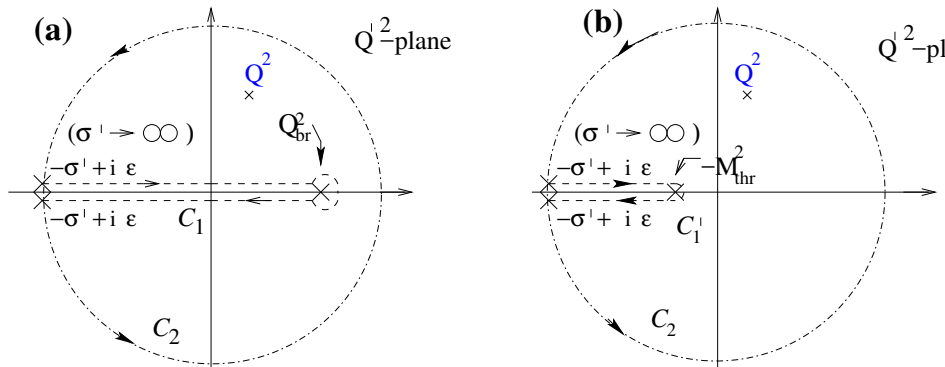
Construction of $\mathcal{A}(Q^2)$

Figure: (a) The contour of integration for the integrand $a(Q'^2)/(Q'^2 - Q^2)$ leading to the dispersion relation (9) for $a(Q^2)$; (b) the contour of integration for the integrand $\mathcal{A}(Q'^2)/(Q'^2 - Q^2)$ leading to the dispersion relation (10). The radius σ' of the circular part tends to infinity.

Construction of $\mathcal{A}(Q^2)$

$$\mathcal{A}(Q^2) = \frac{1}{\pi} \int_{\sigma = M_0^2}^{\infty} \frac{d\sigma \rho_a(\sigma)}{(\sigma + Q^2)} + \Delta\mathcal{A}_{\mathrm{IR}}(Q^2), \qquad (11a)$$

$$\Delta\mathcal{A}_{\mathrm{IR}}(Q^2) = \frac{1}{\pi} \int_{\sigma = M_{\mathrm{thr}}^2}^{M_0^2} \frac{d\sigma \rho_{\mathcal{A}}(\sigma)}{(\sigma + Q^2)} \qquad (11b)$$

$$\Delta\mathcal{A}_{\mathrm{IR}}(Q^2) = [M - 1/M](Q^2) = \frac{\sum_{n=1}^{M-1} A_n Q^{2n}}{\sum_{n=1}^{M} B_n Q^{2n}} \qquad (12a)$$

$$= \sum_{j=1}^{M} \frac{\mathcal{F}_j}{Q^2 + M_j^2} . \qquad (12b)$$

Construction of $\mathcal{A}(Q^2)$

We take $M = 3$:

$$\Delta \mathcal{A}_{\mathrm{IR}}(Q^2) = [2/3](Q^2) = \sum_{j=1}^{3} \frac{\mathcal{F}_j}{Q^2 + M_j^2} \tag{13a}$$

$$\Leftrightarrow \rho_{\mathcal{A}}(\sigma) = \pi \sum_{j=1}^{3} \mathcal{F}_j \, \delta(\sigma - M_j^2) \qquad (0 < \sigma < M_0^2), \tag{13b}$$

This means

$$\rho_{\mathcal{A}}(\sigma) = \pi \sum_{j=1}^{3} \mathcal{F}_j \, \delta(\sigma - M_j^2) + \Theta(\sigma - M_0^2)\rho_a(\sigma) \, . \tag{14}$$

$$\mathcal{A}(Q^2) = \sum_{j=1}^{3} \frac{\mathcal{F}_j}{(Q^2 + M_j^2)} + \frac{1}{\pi} \int_{M_0^2}^{\infty} d\sigma \frac{\rho_a(\sigma)}{(Q^2 + \sigma)} \, . \tag{15}$$

Construction of $\mathcal{A}(Q^2)$

We want at $|Q^2| > 1 \text{ GeV}^2$

$$\mathcal{A}(Q^2) - a(Q^2) \sim \left(\frac{\Lambda_L{}^2}{Q^2}\right)^5 \quad (|Q^2| > \Lambda_L{}^2) . \tag{16}$$

This, and the lattice condition $\mathcal{A}(Q^2) \sim Q^2$ at $Q^2 \to 0$, give 5 conditions

$$-\frac{1}{\pi} \int_{M_0^2}^{\infty} d\sigma \frac{\rho_a(\sigma)}{\sigma} = \sum_{j=1}^{3} \frac{\mathcal{F}_j}{M_j^2} ; \tag{17a}$$

$$\frac{1}{\pi} \int_{-Q_{\text{br}}^2}^{M_0^2} d\sigma \sigma^k \rho_a(\sigma) = \sum_{j=1}^{3} \mathcal{F}_j M_j^{2k} \quad (k = 0, 1, 2, 3) . \tag{17b}$$

Construction of $\mathcal{A}(Q^2)$

But we have 7 parameters, we need 7 conditions, i.e., two more:

1. $Q^2_{\max} \approx 0.135 \text{ GeV}^2$ by lattice calculations, where $\mathcal{A}(Q^2_{\max}) = \mathcal{A}_{\max}$.

2. $\mathcal{A}$-coupling framework should reproduce the approximately correct value of $r_\tau^{(D=0)} \approx 0.20$ (cf. Schael et al. [ALEPH], 2005) where

$$r_{\tau,\text{th}}^{(D=0)} = \frac{1}{2\pi} \int_{-\pi}^{+\pi} d\phi \, (1 + e^{i\phi})^3 (1 - e^{i\phi}) \, d(Q^2 = m_\tau^2 e^{i\phi}; D = 0) \, . \tag{18}$$

Here, $d(Q^2; D = 0)$ is the massless Adler function, $d(Q^2; D = 0) = -1 - 2\pi^2 d\Pi(Q^2; D = 0)/d \ln Q^2$, and its perturbation expansion is known up to $\sim a^4$

$$d(Q^2; D = 0)_{\text{pt}}^{[4]} = a(Q^2) + \sum_{n=1}^{3} d_n a(Q^2)^{n+1}, \tag{19}$$

Construction of $\mathcal{A}(Q^2)$

In our approach, $a(Q^2)^n \mapsto \mathcal{A}_n(Q^2)$ ($\neq \mathcal{A}(Q^2)^n$), (G.C., C. Valenzuela, JPG and PRD, 2006) and

$$d(Q^2; D = 0)^{[4]}_{\mathrm{an}} = \mathcal{A}(Q^2) + d_1 \mathcal{A}_2(Q^2) + d_2 \mathcal{A}_3(Q^2) + d_3 \mathcal{A}_4(Q^2). \quad (20)$$

Nonetheless, another resummation is even more efficient (G.C., 1998; G.C. and R. Kögerler, 2011; G.C. and C. Villavicencio, 2012):

$$d(Q^2; D = 0)^{[4]}_{\mathrm{res}} = \widetilde{\alpha}_1 \, \mathcal{A}(\kappa_1 Q^2) + (1 - \widetilde{\alpha}_1) \, \mathcal{A}(\kappa_2 Q^2) \, . \quad (21)$$

These seven conditions (with $r_{\tau,\mathrm{th}}^{(D=0)} = 0.201$) then give:

$$
\begin{aligned}
M_0^2 &= 8.719 \text{ GeV}^2; \\
M_1^2 = 0.053 \text{ GeV}^2, \quad M_2^2 &= 0.247 \text{ GeV}^2, \quad M_3^2 = 6.341 \text{ GeV}^2; \\
\mathcal{F}_1 = -0.0383 \text{ GeV}^2, \quad \mathcal{F}_2 &= 0.1578 \text{ GeV}^2, \quad \mathcal{F}_3 = 0.0703 \text{ GeV}^2.
\end{aligned}
$$
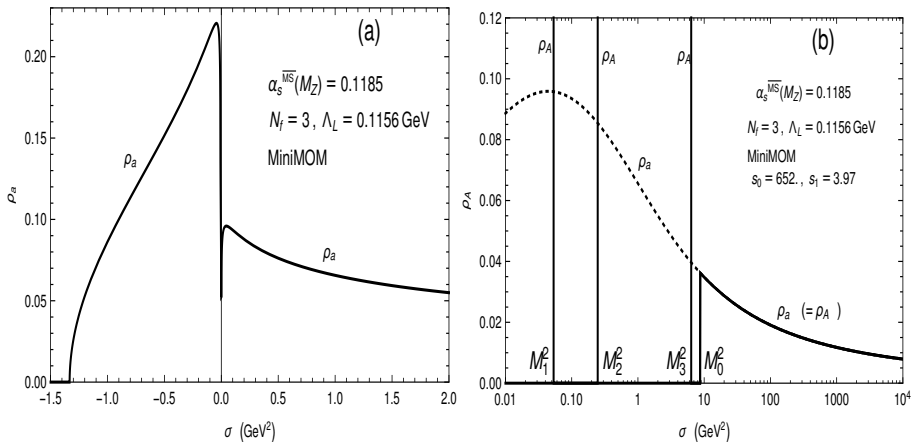
Construction of $\mathcal{A}(Q^2)$

Figure: (a) The spectral function $\rho_a(\sigma) = \text{Im}\, a(Q^2 = -\sigma - i\epsilon)$ for the underlying pQCD coupling in the four-loop Lambert MM scheme, σ is on linear scale; (b) $\rho_{\mathcal{A}}(\sigma) = \text{Im}\, \mathcal{A}(Q^2 = -\sigma - i\epsilon)$ of the considered holomorphic coupling $\mathcal{A}(Q^2)$, $\sigma > 0$ is on logarithmic scale.
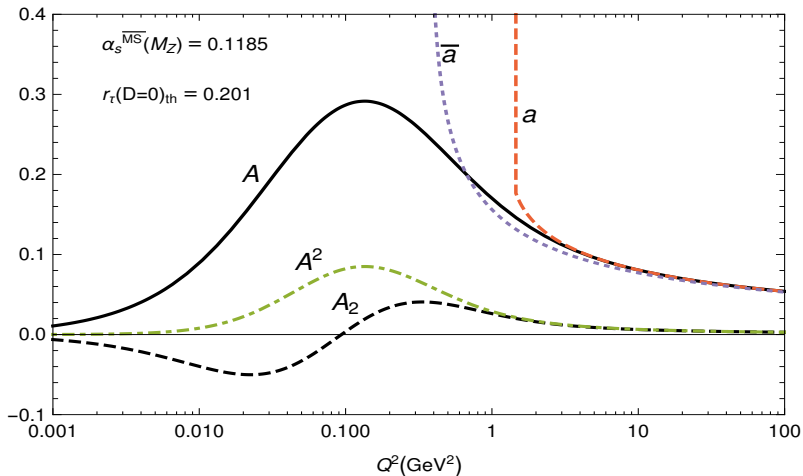
Construction of $\mathcal{A}(Q^2)$

Figure: The considered holomorphic coupling $\mathcal{A}$ at positive Q^2 (solid curve) and its underlying pQCD coupling a (light dashed curve). Included is $\mathcal{A}_2$ (dashed curve) which is the $\mathcal{A}$-analog of power a^2 [cf. Eq. (48)], and the naive (i.e., unusable) power $\mathcal{A}^2$ (dot-dashed curve). Further, the usual $\overline{\text{MS}}$ coupling $\overline{a}$ (dotted curve) is included.

Conclusions

A QCD coupling $\mathcal{A}(Q^2)$ was constructed, in the lattice MiniMOM scheme (rescaled to the usual $\Lambda_{\overline{\text{MS}}}$ scale convention).

1. $\mathcal{A}(Q^2)$ reproduces pQCD results at high momenta $|Q^2| > 1 \; rmGeV^2$.

2. $\mathcal{A}(Q^2) \sim Q^2$ at low momenta $Q^2 \to 0$ ($|Q^2| \lesssim 0.1 \; \text{GeV}^2$), as suggested by high-volume lattice results.

3. $\mathcal{A}(Q^2)$ at intermediate momenta $|Q^2| \sim 1 \; \text{GeV}^2$ reproduces the well measured physics of semihadronic τ-lepton decay.

4. $\mathcal{A}(Q^2)$, as a byproduct of construction, possesses the attractive holomorphic behavior shared by QCD spacelike physical quantities.

The usual $\overline{\text{MS}}$ pQCD coupling $a(Q^2; \overline{\text{MS}}) \equiv \alpha_s(Q^2; \overline{\text{MS}})/\pi$ shares with the coupling $\mathcal{A}$ only the first (high-momentum) property, but on the other three properties it either fails (points 2 and 4) or is considerably worse (point 3).

Appendix 1: Borel sum rules for semihadronic τ decay

$$i \int d^4x \, e^{iq\cdot x} \langle T J_\mu(x) J_\nu(0)^\dagger \rangle = (q_\mu q_\nu - g_{\mu\nu} q^2) \Pi_J^{(1)}(Q^2) + q_\mu q_\nu \Pi_J^{(0)}(Q^2) , \tag{23}$$

where $Q^2 \equiv -q^2$, $J = V, A$, and the quark currents are $J_\mu = \overline{u}\gamma_\mu d$ (when J=V), $J_\mu = \overline{u}\gamma_\mu\gamma_5 d$ (when J=A).

$$\Pi(Q^2) = \Pi_V^{(1)}(Q^2) + \Pi_A^{(1)}(Q^2) + \Pi_{(A)}^{(0)}(Q^2) . \tag{24}$$

Sum rules are:

$$\int_0^{\sigma_{\max}} d\sigma g(-\sigma)\omega_{\exp}(\sigma) = -i\pi \oint_{|Q^2|=\sigma_{\max}} dQ^2 g(Q^2)\Pi_{\text{th}}(Q^2) , \tag{25}$$

where $\sigma_{\max} \leq m_\tau^2$ and $\omega(\sigma)$ is the spectral (discontinuity) function of $\Pi(Q^2)$ along the cut

$$\omega(\sigma) \equiv 2\pi \, \text{Im} \, \Pi(Q^2 = -\sigma - i\epsilon) , \tag{26}$$

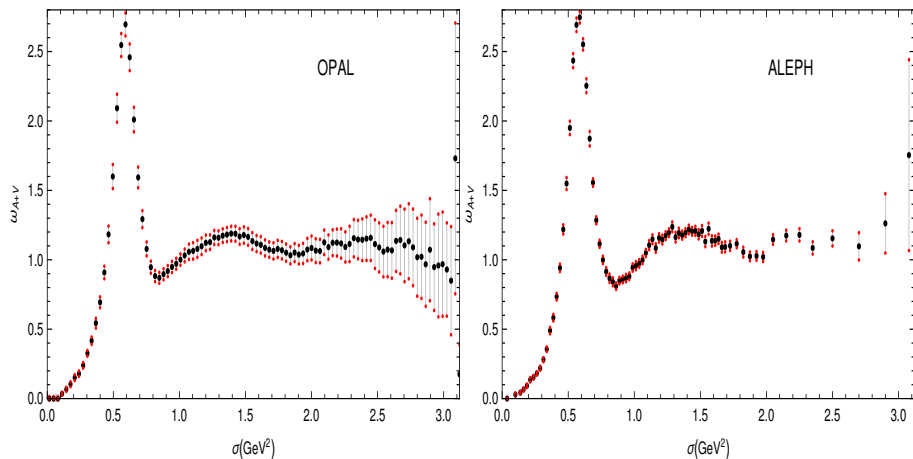# Appendix 1: Borel sum rules for semihadronic τ decay

Figure: (a) The spectral function $\omega_{V+A}(\sigma)$ es measured by OPAL Collaboration
(left-hand figure) and by ALEPH Collaboration (right-hand figure). The pion peak
contribution $2\pi^2 f_\pi^2 \delta(\sigma - m_\pi^2)$ (where $f_\pi = 0.1340$ GeV) must be added to this
(accounting for the pion contribution but without the chiral $m_\pi \neq 0$ effects).

Appendix 1: Borel sum rules for semihadronic τ decay

$$\Pi_{\mathrm{th}}(Q^2) = -\frac{1}{2\pi^2}\ln(Q^2/\mu^2) + \Pi_{\mathrm{th}}(Q^2; D=0) + \sum_{n\geq 2}\frac{\langle O_{2n}\rangle}{(Q^2)^n}\left(1 + \mathcal{C}_n a(Q^2)\right) ,$$

(27)

where $\mathcal{C}_n \approx 0$. Borel sum rules are for the choice

$$g(Q^2) \equiv g_{M^2}(Q^2) = \frac{1}{M^2}\exp(Q^2/M^2) ,$$

(28)

Defining the full Adler function $\mathcal{D}(Q^2)$

$$\mathcal{D}(Q^2) \equiv -2\pi^2\frac{d\Pi_{\mathrm{th}}(Q^2)}{d\ln Q^2} = 1 + d(Q^2; D=0) + 2\pi^2\sum_{n\geq 2}\frac{n\langle O_{2n}\rangle}{(Q^2)^n} .$$

gives the Borel sum rules in the form

$$\frac{1}{M^2}\int_0^{\sigma_{\max}} d\sigma \exp(-\sigma/M^2)\omega_{\exp}(\sigma) = -\frac{i}{2\pi}\int_{\phi=-\pi}^{\pi}\frac{dQ^2}{Q^2}\mathcal{D}(Q^2)\big[e^{Q^2/M^2}$$
$$-e^{-\sigma_{\max}/M^2}\big]\big|_{Q^2=\sigma_{\max}\exp(i\phi)} .$$

Hence, the Borel sum rule has the form

$$\mathrm{Re}B_{\mathrm{exp}}(M^2) = \mathrm{Re}B_{\mathrm{th}}(M^2) \; , \qquad (29)$$

$$
\begin{aligned}
\text{where}: \quad B_{\mathrm{exp}}(M^2) &\equiv \int_0^{\sigma_{\mathrm{max}}} \frac{d\sigma}{M^2} \, \exp(-\sigma/M^2)\omega_{\mathrm{exp}}(\sigma)_{V+A} \; , \\
B_{\mathrm{th}}(M^2) &\equiv \left(1 - \exp(-\sigma_{\mathrm{max}}/M^2)\right) + B_{\mathrm{th}}(M^2; D\!=\!0) \\
&\quad + 2\pi^2 \sum_{n \geq 2} \frac{\langle O_{2n} \rangle}{(n-1)! \, (M^2)^n} \; ,
\end{aligned}
\qquad (30a)
$$

where the leading-twist contributions ($D = 0$) is

$$
\begin{aligned}
B_{\mathrm{th}}(M^2; D\!=\!0) &= \frac{1}{2\pi} \int_{-\pi}^{\pi} d\phi \, d(Q^2 = \sigma_{\mathrm{max}}e^{i\phi}; D=0)\left[\exp\left(\frac{\sigma_{\mathrm{max}}e^{i\phi}}{M^2}\right)\right. \\
&\quad \left. - \exp\left(-\frac{\sigma_{\mathrm{max}}}{M^2}\right) \right].
\end{aligned}
\qquad (31)
$$

Appendix 1: Borel sum rules for semihadronic τ decay

The Borel scale M^2 is taken along rays in the complex M^2-plane which we will choose as:

$$M^2 = |M^2| \exp(i\Psi), \quad 0.65\,\mathrm{GeV}^2 \leq |M^2| \leq 1.50\,\mathrm{GeV}^2, \quad \Psi = \pi/6, \pi/4, 0.$$
(32)

1. At low Borel scales M^2 the Borel transform $B(M^2)$ probes the low-σ (IR) regime. On the other hand, the high-σ (UV) contributions have larger experimental uncertainties $\delta\omega(\sigma)$ and are suppressed in the Borel transform.

2. When $M^2 = |M^2| \exp(i\pi/6)$, it is straightforward to see that the $D = 6$ term in $\mathrm{Re}B_{\mathrm{th}}(M^2)$ is zero (and thus only the $D = 4$ higher-twist term survives). Analogously, when $M^2 = |M^2| \exp(i\pi/4)$, the $D = 4$ term in $\mathrm{Re}\,B_{\mathrm{th}}(M^2)$ is zero (and thus only the $D = 6$ higher-twist term survives). This helps us extract more easily the values of the condensates $\langle O_4 \rangle = (1/6)\langle aGG \rangle$ and $\langle O_6 \rangle$ for $M^2 = |M^2| \exp(i\pi/6), |M^2| \exp(i\pi/4)$, respectively.
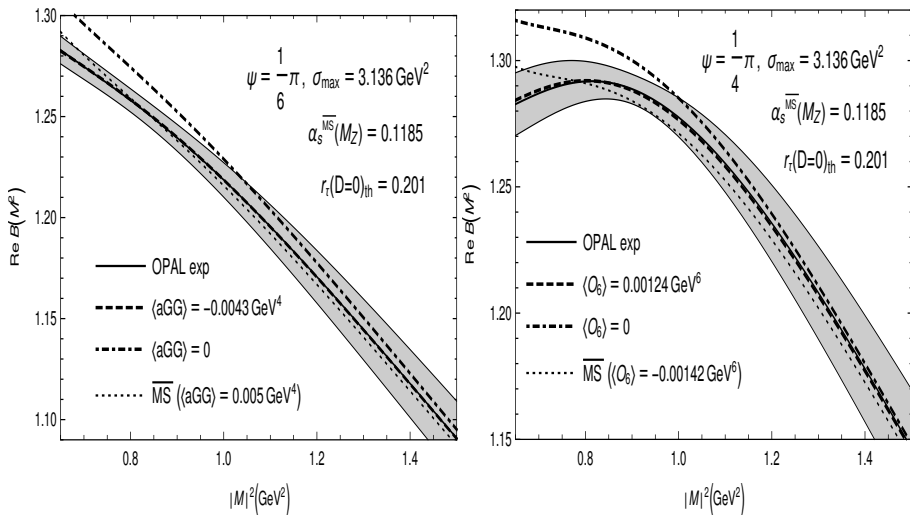
Appendix 1: Borel sum rules for semihadronic τ decay

Figure: Borel transforms $\mathrm{Re}\,B(M^2)$ along the rays $M^2 = |M^2|\exp(i\Psi)$ with $\Psi = \pi/6$ (left-hand side) and $\Psi = \pi/4$ (right-hand side), as a function of $|M^2|$.

Appendix 1: Borel sum rules for semihadronic τ decay

$$\langle aGG \rangle = (-0.0068 \pm 0.0017) \text{ GeV}^4 \tag{33a}$$
$$\chi^2 = 1.1 \times 10^{-6}; \chi^2_{\exp} = 1.4 \times 10^{-4},$$
$$\langle O_6 \rangle_{V+A} = (+0.0013 \pm 0.0003) \text{ GeV}^6 \tag{33b}$$
$$\chi^2 = 6.7 \times 10^{-7}; \chi^2_{\exp} = 2.0 \times 10^{-4}.$$

$$\langle aGG \rangle_{\overline{\text{MS}}} = (+0.0025 \pm 0.0017) \text{ GeV}^4 \tag{34a}$$
$$\chi^2_{\overline{\text{MS}}} = 7.2 \times 10^{-6},$$
$$\langle O_6 \rangle_{V+A,\overline{\text{MS}}} = (-0.0014 \pm 0.0003) \text{ GeV}^6 \tag{34b}$$
$$\chi^2_{\overline{\text{MS}}} = 2.5 \times 10^{-5}.$$

Appendix 1: Borel sum rules for semihadronic τ decay

$\psi = 0$, $\sigma_{\max} = 3.136\,\mathrm{GeV}^2$

$\alpha_s^{\overline{\mathrm{MS}}}(M_Z) = 0.1185$

$r_\tau(D=0)_{\mathrm{th}} = 0.201$

OPAL exp

AQCD

AQCD $\langle aGG \rangle = 0 = \langle O_6 \rangle$
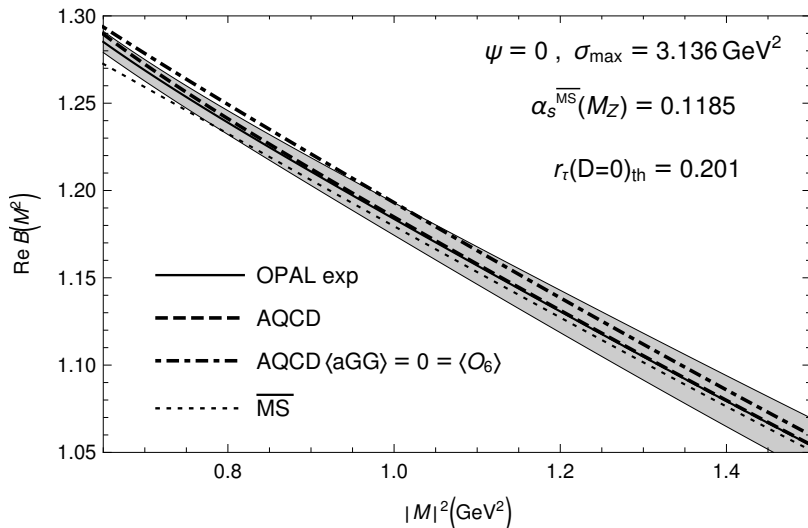
$\overline{\mathrm{MS}}$

Figure: Analogous to the previous Figures, but now the Borel transforms $B(M^2)$ are for real $M^2 > 0$.

Appendix 1: Borel sum rules for semihadronic τ decay

$$\Psi = 0 : \; \chi^2 = 2.1 \times 10^{-6}, \quad \chi^2_{\overline{\text{MS}}} = 3.3 \times 10^{-5} \quad (\chi^2_{\text{exp}} = 1.2 \times 10^{-4}) . \quad (35)$$

Cross-check with $r_\tau^{(D=0)}$:

$$
\begin{aligned}
r_{\tau,\text{exp}}^{(D=0)} &= 2 \int_0^{\sigma_{\max}} \frac{d\sigma}{m_\tau^2} \left(1 - \frac{\sigma}{m_\tau^2}\right)^2 \left(1 + 2\frac{\sigma}{m_\tau^2}\right) \omega_{\text{exp}}(\sigma) - 1 \\
&\quad + 12\pi^2 \frac{\langle O_6 \rangle_{V+A}}{m_\tau^6} \\
&\approx (0.198 \pm 0.006) + 0.005 = 0.203 \pm 0.006 .
\end{aligned}
$$

In the $\overline{\text{MS}}$ case, this type of consistency is lost, because in this case $\langle O_6 \rangle_{V+A} = -0.0014 \; \text{GeV}^6$ and thus $r_{\tau,\text{exp},\overline{\text{MS}}}^{(D=0)} = (0.198 \pm 0.006) - 0.005 = 0.193 \pm 0.006$, this differing by about two standard deviations from the theoretical value in the $\overline{\text{MS}}$ approach, $r_{\tau,\text{th}}^{(D=0)}(d_{pt,\overline{\text{MS}}}^{[4]}) = 0.182$.

Appendix 2: V-channel Adler function

$$
\begin{aligned}
\mathcal{D}_V(Q^2) &\equiv -4\pi^2 \frac{d\Pi_V(Q^2)}{d \ln Q^2} \\
&= 1 + d(Q^2; D=0) + 2\pi^2 \sum_{n \geq 2} \frac{n2\langle O_{2n}\rangle_V}{(Q^2)^n}. \quad (37)
\end{aligned}
$$

Here

$$
2\langle O_4 \rangle_V = 2\langle O_4 \rangle_A = \langle O_4 \rangle_{V+A} . \quad (38)
$$

The factorization hypothesis gives

$$
\langle O_6 \rangle_V \approx -\frac{7}{4}\langle O_6 \rangle_{V+A}, \quad (39)
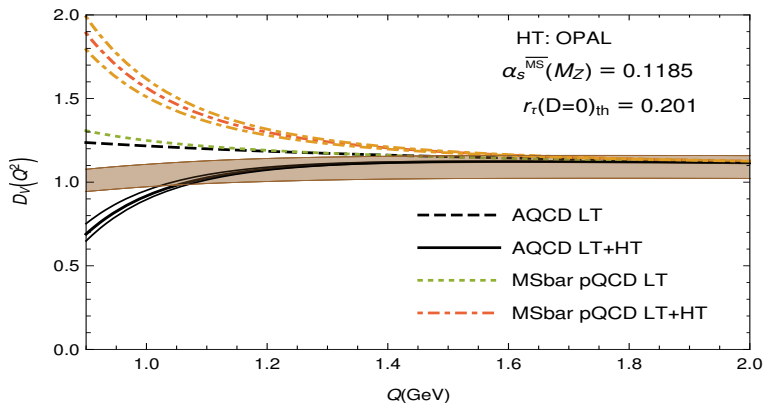$$

Appendix 2: V-channel Adler function

Figure: The V-channel Adler function at $Q^2 > 0$ ($Q \equiv \sqrt{Q^2}$): the brown band are the experimental values (A.V. Nesterenko, 2016, Fig. 1.7 there). The solid lines are the theoretical curves for $\alpha_s(M_Z^2) = 0.1181$ (upper), 0.1185 (middle), 0.1189 (lower curve) in the $\mathcal{A}$QCD+OPE approach, and the dash-dotted lines are in the $\overline{\rm MS}$ pQCD+OPE approach. The dashed line is the leading twist (LT) contribution in $\mathcal{A}$QCD, and the dotted line in $\overline{\rm MS}$ pQCD, for $\alpha_s(M_Z^2) = 0.1185$. The $D = 4$ and $D = 6$ terms (higher-twist) are with the corresponding values of the condensates as explained in the text. $N_f = 3$ is used throughout.

Massive Adler approach ($m\mathcal{A}QCD$):

$$
\begin{aligned}
\mathcal{D}_V(Q^2)_{m\mathcal{A}QCD} &= \mathcal{D}^{(0)}(Q^2)_m \\
&+ \frac{Q^2}{(Q^2+m^2)}\frac{1}{\pi}\int_{m^2}^{+\infty}d\sigma\left(1-\frac{m^2}{\sigma}\right)\frac{\rho_d(\sigma)}{(\sigma+Q^2)}, \quad (40)
\end{aligned}
$$

where $m = 2m_\pi$ kinematic threshold (cf. A.V. Nesterenko 2015), and the leading order term is

$$
\begin{aligned}
\mathcal{D}^{(0)}(Q^2)_m &= 1 + \frac{3}{z^2}\left[1+\left(1+\frac{1}{z^2}\right)^{1/2}\mathrm{ArcSinh}(z)\right]\Bigg|_{z=\sqrt{Q^2}/m} \quad (41a) \\
&= \frac{2}{5}z^2 - \frac{8}{35}z^4 + \frac{16}{105}z^6 + \ldots\Bigg|_{z^2=Q^2/m^2}, \quad (41b)
\end{aligned}
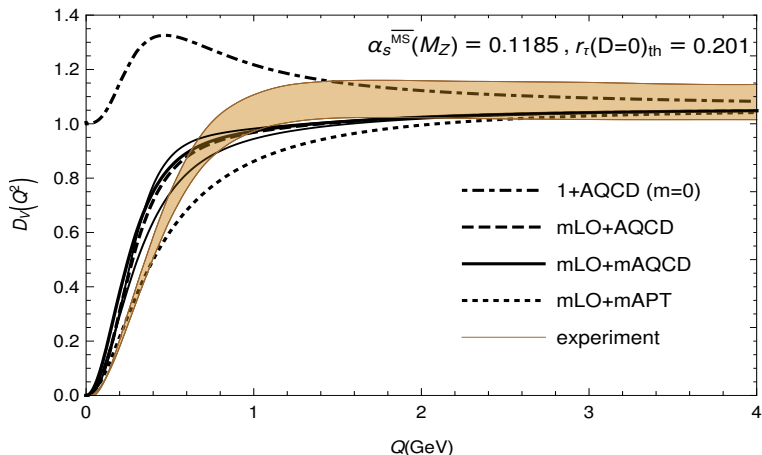$$

Appendix 2: V-channel Adler function

Figure: The V-channel Adler function at $Q^2 > 0$ ($Q \equiv \sqrt{Q^2}$): the brown band are the experimental values as in the previous Figure. The three solid lines are the theoretical curves for $\alpha_s(M_Z^2) = 0.1189$ (upper), 0.1185 (middle), 0.1181 (lower curve) in the massive $\mathcal{A}$QCD approach (mLO+m$\mathcal{A}$QCD). The dash-dotted line is the massless limit ($m^2 \mapsto 0$), for $\alpha_s(M_Z^2) = 0.1185$. The dashed line is for the massive leading order term $\mathcal{D}_V^{(0)}(Q^2)_m$ and massless $\mathcal{A}$QCD term (mLO+$\mathcal{A}$QCD), for $\alpha_s(M_Z^2) = 0.1185$. The dotted line (mLO+mAPT) is the case where $\rho_d(\sigma)$ in Eq. (40) is the pQCD spectral function, as explained in the text. $N_f = 3$ is used throughout for $\rho_d(\sigma)$.

Appendix 3: Higher power analogs

The analytic version $(a^n)_{\mathrm{an}} = \mathcal{A}_n$ of the analogs of higher powers a^n of the (underlying) pQCD coupling, for integer n, was constructed in the general case of holomophic QCD (G.C.and C. Valenzuela, 2006, JPG and PRD). We recapitulate it briefly here. The construction goes via a detour by considering first, instead of the powers a^n, the logarithmic derivatives

$$\widetilde{a}_{n+1}(Q^2) \equiv \frac{(-1)^n}{\beta_0^n n!} \frac{\partial^n a(Q^2)}{\partial(\ln Q^2)^n} , \qquad (n = 1, 2, \ldots) . \qquad (42)$$

According to RGE, we have $\widetilde{a}_{n+1}(Q^2) = a(Q^2)^{n+1} + \mathcal{O}(a^{n+2})$.

Specifically, we have

$$
\begin{aligned}
\widetilde{a}_2 &= a^2 + c_1 a^3 + c_2 a^4 + \cdots , & (43)\\
\widetilde{a}_3 &= a^3 + \frac{5}{2} c_1 a^4 + \cdots , \qquad \widetilde{a}_4 = a^4 + \cdots , \qquad \text{etc.} . & (44)
\end{aligned}
$$

Inverting these relations gives

$$
a^2 = \widetilde{a}_2 - c_1 \widetilde{a}_3 + \left(\frac{5}{2} c_1^2 - c_2 \right) \widetilde{a}_4 + \cdots , \tag{45}
$$

$$
a^3 = \widetilde{a}_3 - \frac{5}{2} c_1 \widetilde{a}_4 + \cdots , \qquad a^4 = \widetilde{a}_4 + \cdots , \qquad \text{etc.} \tag{46}
$$

Appendix 3: Higher power analogs

The linearity of "analytization" implies that in holomorphic QCD the correponding analogs of logarithmic derivatives are constructed in the very same way

$$\widetilde{\mathcal{A}}_{n+1}(Q^2) \equiv \frac{(-1)^n}{\beta_0^n n!} \frac{\partial^n \mathcal{A}(Q^2)}{\partial(\ln Q^2)^n} \ . \qquad (n = 1, 2, \ldots) \ . \tag{47}$$

Further, the linearity of the relations (46) implies that the analogs $\mathcal{A}_2$, $\mathcal{A}_3$, $\mathcal{A}_4$ of the powers a^n are obtained in the same way

$$\mathcal{A}_2 \equiv \left(a^2\right)_{\mathrm{an}} = \widetilde{\mathcal{A}}_2 - c_1\widetilde{\mathcal{A}}_3 + \left(\frac{5}{2}c_1^2 - c_2\right)\widetilde{\mathcal{A}}_4 + \cdots \ , \tag{48}$$

$$\mathcal{A}_3 \equiv \left(a^3\right)_{\mathrm{an}} = \widetilde{\mathcal{A}}_3 - \frac{5}{2}c_1\widetilde{\mathcal{A}}_4 + \cdots \ , \quad \mathcal{A}_4 \equiv \left(a^4\right)_{\mathrm{an}} = \widetilde{\mathcal{A}}_4 + \cdots \tag{49}$$

etc. For TPS $d^{[4]}$, we truncate the above relations at $\widetilde{\mathcal{A}}_4$ (including $\widetilde{\mathcal{A}}_4$).